Numerical simulation of the heavily Ge-doped polarization-maintaining fiber with normal dispersion*

LI Hongwei, WANG Chuncan, and AN Haitao**

Key Laboratory of All Optical Network and Advanced Telecommunication Network, Ministry of Education, Institute of Lightwave Technology, Beijing Jiaotong University, Beijing 100044, China

(Received 11 March 2021; Revised 22 April 2021)

The heavily germanium (Ge)-doped silica fiber assisted by two air holes in the cladding exhibits high nonlinearity and birefringence, low loss and normal group velocity dispersion (GVD) for two fundamental modes (FMs). When the 1 920 nm and 0.1 ps pump pulse with 100 kW peak power is coupled into the 0.5-m-long fiber and polarized along one of two principle axes, the generated spectra can cover the wavelength range around 1 000—2 500 nm at −20 dB. Furthermore, the output pulse has an excellent coherence in the whole wavelength range.

Document code: A **Article ID:** 1673-1905(2022)01-0035-8

DOI https://doi.org/10.1007/s11801-022-1031-z

Supercontinuum (SC) generation (SCG) refers to the process of spectral broadening under the effects of fiber dispersion and nonlinearity, which has been attracting great research interest because of its extensive applications in optical coherence tomography[1], biomedicine[2], biophotonic[3], and spectroscopy[4]. The all-normal dispersion (ANDi) optical fibers have recently emerged as attractive platforms to improve the noise and coherence performance of SC generation compared to anomalous SC generation. The ANDi property can be obtained by using the photonic crystal fibers (PCFs) based on the soft-glass[5], silica[6], chalcogenide-glass[7] and tellurite-glass[8], hollow-core fibers filled with highly nonlinear liquid[9] and heavily germanium (Ge)-doped silica fiber[10].

Furthermore, compared to the SCG based on the non-polarization-maintaining (PM) fibers, the SCG with a higher degree of polarization can be obtained by using the PM fibers because that the polarization instabilities caused by the nonlinear coupling among the randomly polarized modes in the fibers can be suppressed[11]. Consequently, the linearly polarized SC with high coherence can be obtained by using the air-silica PM PCFs[11-13] soft-glass PM PCF with stress-inducing elements[14], $As_{38}Se_{62}$-glass PM PCF[15], silica-based highly nonlinear PCF with 50 mol% GeO_2-doped core[16], and single-polarization CS_2-core silica fiber assisted by two gold wires[17].

Since the Ge-doped silica fiber is more compatible with fusion splicing to the other silica fiber compared with the soft-glass-based fibers, it is interesting to investigate the properties of the silica-based PM fiber. In this paper, the heavily Ge-doped PM fiber is proposed to obtain both high nonlinearity and high birefringence. Compared with the PM PCF[11-16], the proposed PM fiber has more simple structure and flat group velocity dispersion (GVD) profiles in the wavelength range of 1 400—2 600 nm. The fiber structure and theoretical model are presented, and the fiber properties, including dispersion, nonlinear parameter, birefringence and loss are discussed in the wavelength range from 1 000 nm to 3 000 nm. The SCG based on the Ge-doped PM fiber is investigated by numerical simulation.

As shown in Fig.1(a), the zero dispersion wavelength (ZDW) of the Ge-doped silica shifts toward longer wavelength side with an increase of the Ge concentration X. When X=100 mol% (red curve), the corresponding ZDW is 1 730 nm, which is located 470 nm away from the ZDW of the pure silica (black curve). Additionally, it can be seen in Fig.1(b) that the refractive index difference between the Ge-doped silica and pure silica can reach up to 0.14 in the wavelength range from 1 000 nm to 3 000 nm. Fig.2 shows the cross section of the proposed PM fiber, where two air holes lie symmetrically in the cladding for the purpose of introducing the birefringence. The horizontal and vertical directions are defined as the x- and y-axes, respectively. The GVD profiles of the fiber can be designed by changing values of Λ, r_1, r_2 and X.

In Fig.2, the parameter n_C representing the refractive index of air, is set to 1. The parameters n_A and n_B represent the refractive indices of GeO_2-doped silica and pure silica[18], which are given by

$$n^2_{\mathrm{A\,or\,B}}(\lambda)-1=\sum_1^3\frac{[SA_i+X(GA_i-SA_i)]\lambda^2}{\lambda^2-[SI_i+X(GI_i-SI_i)]^2}\,, \tag{1}$$

where SA_i, SI_i, GA_i and GI_i (i = 1, 2, 3) are the Sellmeier coefficients for pure silica and GeO_2-doped silica glass. λ

* This work has been supported by the National Natural Science Foundation of China (No.61575018).

** E-mail: chcwang@bjtu.edu.cn

is the wavelength in the vacuum, and X is the mole fraction of GeO_2 in mol%. When X=0, the refractive index in Eq.(1) is n_B. The GVD $D(\lambda)$ can be written as

$$D(\lambda)=-\frac{\lambda}{c}\frac{\mathrm{d}^2 n_{\mathrm{eff}}(\lambda)}{\mathrm{d}\lambda^2}, \tag{2}$$

where c is the speed of light in vacuum, $n_{\mathrm{eff}}(\lambda)$ is the effective index of the fundamental mode (FM) at the operating wavelength λ, which can be obtained by solving the wave equation with the commercial software Comsol. The nonlinearity parameter $\gamma(\lambda)$ can be defined as[10]

$$\gamma(\lambda)=\frac{2\pi}{\lambda}\frac{\iint_{-\infty}^{\infty} n_2(x,y)\left|F(x,y)\right|^4 \mathrm{d}x\mathrm{d}y}{\left(\iint_{-\infty}^{\infty}\left|F(x,y)\right|^2 \mathrm{d}x\mathrm{d}y\right)^2}, \tag{3}$$

where $n_2(x, y)$ is the nonlinearity refractive index (NRI), and $F(x, y)$ is the modal intensity distribution of the fiber mode. The NRI n_2 of GeO_2-doped silica and pure silica are given by (2.16+0.033X) with the unit of 10^{-20} $\mathrm{m^2/W}$[19]. The birefringence parameter B is defined as

$$B=\left|n_{\mathrm{eff}}^{x}-n_{\mathrm{eff}}^{y}\right|, \tag{4}$$

where n^x_{eff} and n^y_{eff} are the effective refractive indices of the FMs polarized along x- and y-axes, respectively. The total loss L of the optical mode is the sum of the confinement loss L_C and the absorption loss L_A, which can be calculated by

$$L_C(\lambda)=\frac{20}{\ln(10)}\frac{2\pi}{\lambda}\mathrm{Im}(n_{\mathrm{eff}}), \tag{5}$$

$$L_A=\Gamma^{\mathrm{core}}(\lambda)\times\alpha_{\mathrm{GeO2}}+\Gamma^{\mathrm{cladding}}(\lambda)\times\alpha_{\mathrm{SiO2}}, \tag{6}$$

where $\mathrm{Im}(n_{\mathrm{eff}})$ is the imaginary part of n_{eff}. $\Gamma^{\mathrm{core}}(\lambda)$ and $\Gamma^{\mathrm{cladding}}(\lambda)$ represent the ratios of modal intensities in the regions of core and cladding, respectively. α_{GeO2} and α_{SiO2} are the absorption losses of Ge-doped silica and pure silica, respectively[20].

As shown in Fig.3(a), the proposed PM fiber exhibits more flat normal GVD profiles over the wavelength range of 1 500—2 500 nm than that of the Ge-doped fiber without air holes in the cladding. The GVD values are −8 ps/nm·km and −14 ps/nm·km near 1 920 nm for the x- and y-polarized FMs. Additionally, as shown in Fig.3(b), the group velocity (GV) for the y-polarized FM is relatively higher than that for the x-polarized FM. Consequently, the polarization directions along x- and y-axes correspond to slow and fast axes, respectively. It can be seen in Fig.3(c) that the birefringence of the PM fiber increases with wavelength, where the birefringence is more than 1×10^{-4} at 1 920 nm.

First, as shown in Fig.4, the birefringence B decreases with an increase of Λ. As a result, the GVD profiles of two FMs are downshifted and close to those of non-PM fiber. When Λ is < 3.4 μm, GVD values in the region beyond 2 500 nm decrease due to the large waveguide dispersion. However, GVD profiles become narrow at Λ=3.0 μm, and have two ZDMs for the FM with the polarization along x-axis. When Λ decreases from 3.8 μm to 3.0 μm, the birefringence at 1 920 nm increases from 0.5×10^{-4} to 3×10^{-4}, while GVD values of FMs with the polarization directions along x- and y-axes at 1 920 nm increase from −18 ps/nm·km and −22 ps/nm·km to 4 ps/nm·km and −4 ps/nm·km, respectively, and the dispersion slope values near 1 900 nm are in the range of −0.015—0.005 ps/nm^2·km.

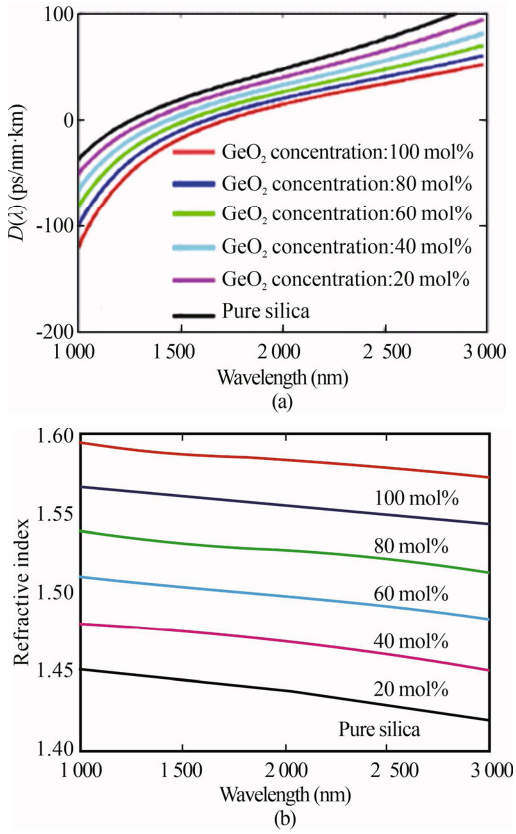

Fig.1 The curves of (a) material dispersions and (b) refractive indices for pure silica and GeO_2-doped silica with different Ge concentrations

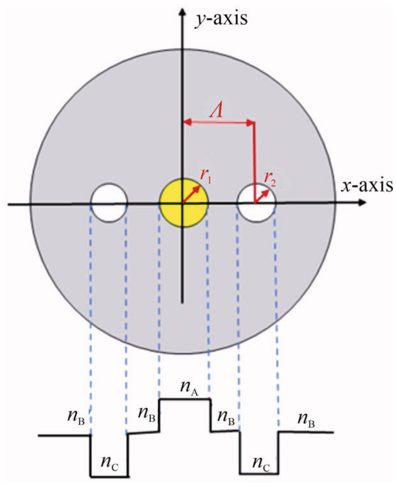

Fig.2 Structure of the proposed PM fiber, where the cladding material is pure silica, the core with the radius r_1 is made of Ge-doped silica, two air holes with the radius r_2 lie on opposite sides of the core symmetrically along the x-axis, and Λ is the core-to-air-hole spacing

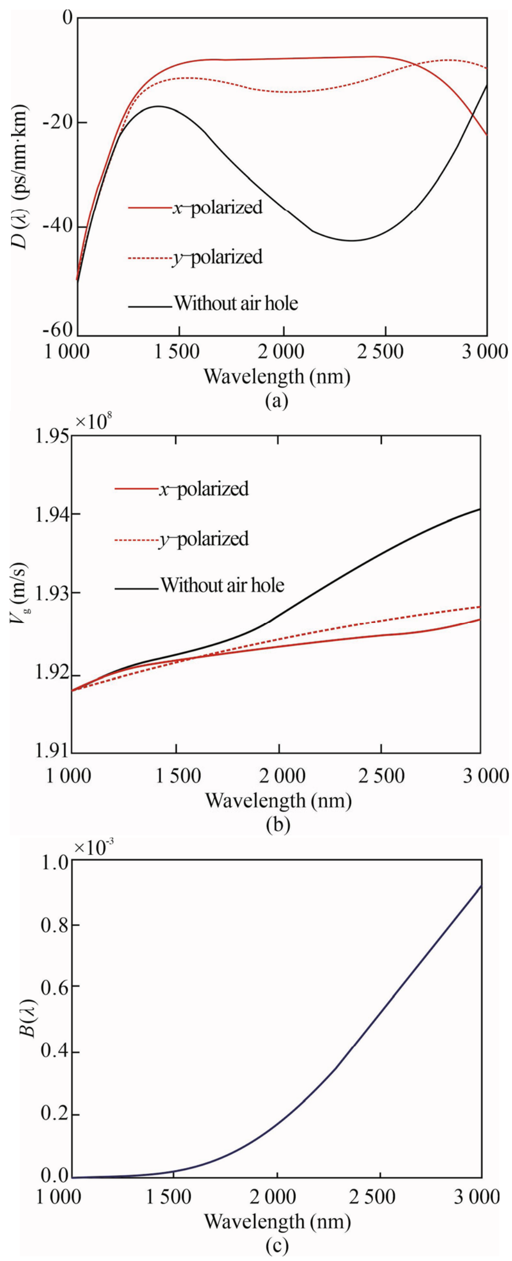

Fig.3 The fiber properties for the *x*- and *y*-polarized FMs including (a) GVD, (b) GV and (c) birefringence, where r_1=1.2 μm, r_2=1.0 μm, Λ=3.4 μm and X=60 mol%

Second, as shown in Fig.5, for the proposed PM fibers with r_2 values of 1.0 μm, 1.2 μm or 1.4 μm, both *x*- and *y*-polarized FMs exhibit the normal GVD profiles in the wavelength range of 1 000 nm to 3 000 nm. However, the SC generation under the condition of r_2=1.0 μm is desired due to its flat GVD profiles and high birefringence. For this reason, we assume r_2=1.0 μm in the following discussion. Furthermore, Fig.6 shows the fiber GVD and birefringence with different values of r_1. The GVD profiles exhibit much larger variations compared to those in Figs.4 and 5. The result indicates that the parameter r_1 should be carefully tuned for obtaining a desired GVD property. When r_1 increases from 0.8 μm to 1.4 μm, GVD values at 1 920 nm for FMs polarized along *x*- and *y*-axes increase from −115 ps/nm·km and −118 ps/nm·km to 21 ps/nm·km and 16 ps/nm·km, respectively. Moreover, in all cases the birefringence values at 1 920 nm are more than 1×10^{-4}, which indicates the proposed PM fiber has the high birefringence.

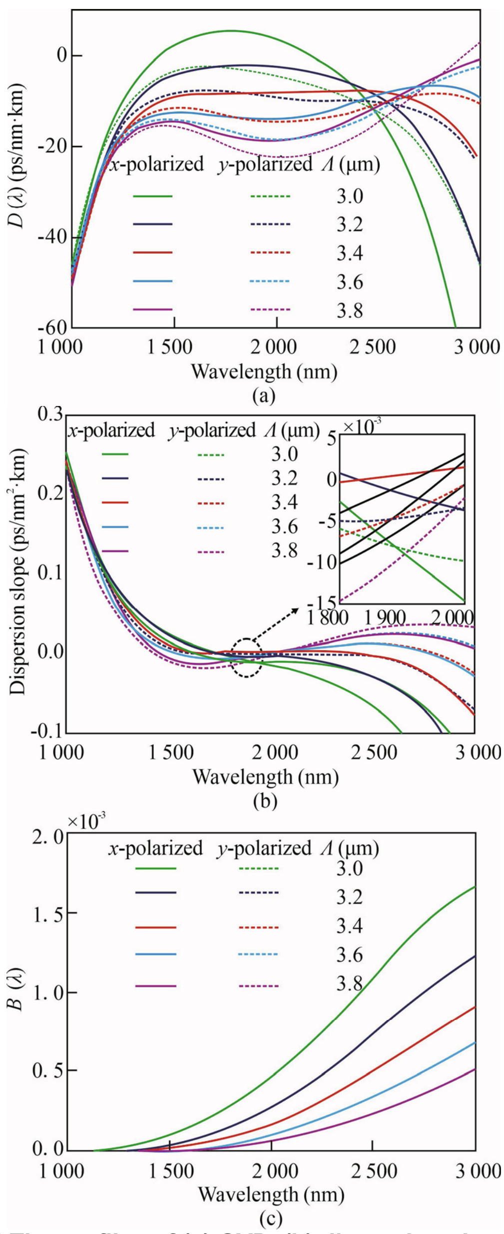

Fig.4 The profiles of (a) GVD, (b) dispersion slope and (c) birefringence for two FMs in the proposed PM fiber, where Λ values are 3.0 μm, 3.2 μm, 3.4 μm, 3.6 μm and 3.8 μm, where r_1=1.2 μm, r_2=1.0 μm and X=60 mol%

Finally, the influences of the concentration X on the GVD and birefringence are shown in Fig.7. It can be seen that the PM fiber with X=60 mol% exhibits a wide and flat normal GVD profile. When X=20 mol%, the birefringence reaches its maximum value at 1 850 nm. However, when X=60 mol%, the birefringence at 1 920 nm is as high as 1.6×10^{-4}. As a result, we assume r_1=1.2 μm, r_2=1.0 μm, Λ=3.4 μm and X=60 mol% in the following discussion due to its wide and flatted GVD curves combined with the relatively high birefringence.

As shown in Fig.8(a), the total losses of the PM fiber are much lower than 0.01 dB/cm in the whole wavelength range from 1 000 nm to 2 500 nm. Moreover, as shown in Fig.8(b), the nonlinear parameters and effective mode areas over the wavelength range of 1 000—3 000 nm are almost identical for two FMs, while γ can reach 0.01 W^{-1}/m at 1 920 nm.

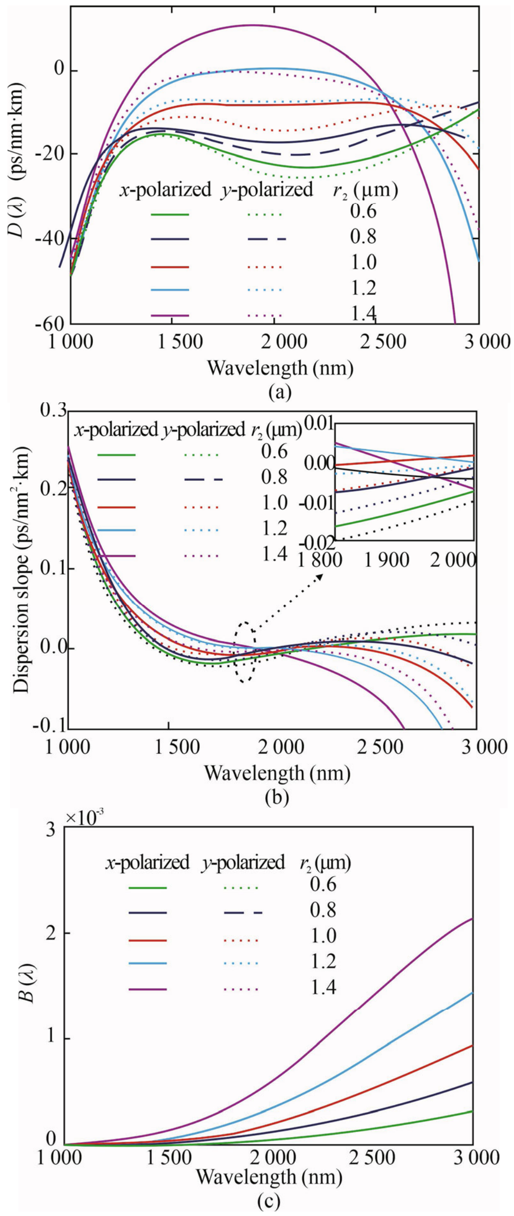

Fig.5 The curves of (a) GVD, (b) dispersion slope and (c) birefringence for FMs polarized along *x*- and *y*-axes in the proposed PM fibers with r_2 values of 0.6 μm, 0.8 μm, 1.0 μm, 1.2 μm and 1.4 μm, where r_1=1.2 μm, *Λ*=3.4 μm and *X*=60 mol%

When the coupling effect between the *x*- and *y*-polarized modes is considered, the pulse varying envelopes in each polarization direction of the PM fiber satisfy the coupled generalized nonlinear Schrödinger equations (GNLSEs) as[21]

$$\frac{\partial \tilde{A}_x(z,\Omega)}{\partial z}=[\mathrm{i}\tilde{\beta}^{(x)}(\omega)-\frac{\alpha^{(x)}(\omega)}{2}]\tilde{A}_x(z,\Omega)+\mathrm{i}\gamma(\omega)\left(1+\frac{\Omega}{\omega_0}\right)F[(1-f_R)A_x(T)(|A_x(T)|^2+\frac{2}{3}|A_y(T)|^2)+f_R A_x(T)h(\omega)\times|A_x(T)|^2+(1-f_R)\frac{1}{3}A_x^*(T)A_y^2(T)\mathrm{e}^{-2\mathrm{i}\Delta\beta z}], \quad (7)$$

$$\frac{\partial \tilde{A}_y(z,\Omega)}{\partial z}=[\mathrm{i}\tilde{\beta}^{(y)}(\omega)-\frac{\alpha^{(y)}(\omega)}{2}]\tilde{A}_y(z,\Omega)+\mathrm{i}\gamma(\omega)\left(1+\frac{\Omega}{\omega_0}\right)F[(1-f_R)A_y(T)(|A_y(T)|^2+\frac{2}{3}|A_x(T)|^2)+f_R A_y(T)h(\omega)\times|A_y(T)|^2+(1-f_R)\frac{1}{3}A_y^*(T)A_x^2(T)\mathrm{e}^{2\mathrm{i}\Delta\beta z}], \quad (8)$$

where $\tilde{A}_x(z,\Omega)$ and $\tilde{A}_y(z,\Omega)$ represent the slowly varying pulse amplitudes in the frequency domain, which are the Fourier transform of $A_x(z,T)$ and $A_y(z,T)$, where x and y represent the polarization directions along *x*- and *y*-axes, respectively. $\alpha^{(x)}(\omega)$ and $\alpha^{(y)}(\omega)$ are the total losses of *x*- and *y*-polarized axes, respectively. $\tilde{\beta}^{(x)}(\omega)$ and $\tilde{\beta}^{(y)}(\omega)$ are the dispersion coefficients in the polarization directions along *x*- and *y*-axes, respectively. $\gamma(\omega)$ is the nonlinear parameter and ω_0 is the center frequency. $\Delta\beta=(2\pi/\lambda)B=2\pi/L_B$, where L_B represents the beat length. Here, we assume the input pulse is a Gaussian pulse, i.e., $A(0,T)=\sqrt{P_0}\exp(-T^2/2T_0^2)$, where P_0 is the peak power, and $T_0=T_{FWHM}/\sqrt{2\ln 2}$; T_{FWHM} represents the full width at half-maximum pulse duration. The difference of group velocities between two polarization components can prevent their nonlinear coupling due to a large enough time delay. This feature can be characterized by the walk-off term $\beta_{1y}(\omega_0)-\beta_{1x}(\omega_0)$ with the walk-off length $L_W=T_0/|\beta_{1y}(\omega_0)-\beta_{1x}(\omega_0)|$. $h(\omega)$ is the Raman response function, whose corresponding time domain is $h(T)=(1-f_R)\delta(T)+f_R h_R(T)$, including both instantaneous and delayed Raman contributions. The fractional contribution of the delayed Raman response to nonlinear polarization f_R is 0.18. The Raman response term is given by[22]

$$h_R(T)=\frac{\tau_s^2+\tau_v^2}{\tau_s\tau_v}\exp(-T/\tau_v)\sin(T/\tau_s)\Theta(T), \quad (9)$$

where τ_s and τ_v are taken to be 12.2 fs and 83 fs, respectively. $\Theta(T)$ is Heaviside step function.

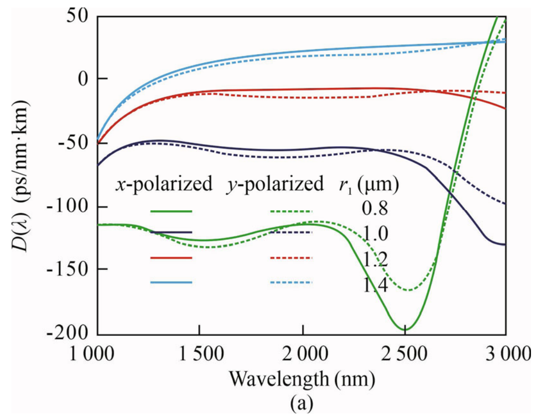

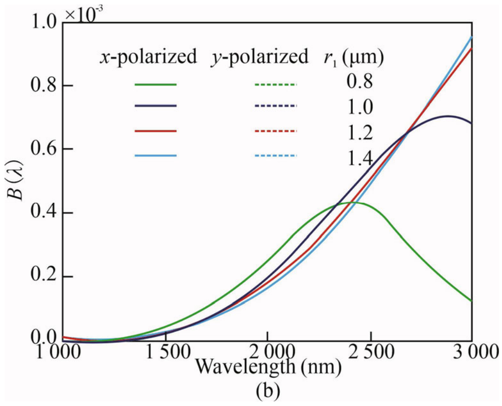

Fig.6 The curves of (a) GVD and (b) birefringence for FMs polarized along *x*- and *y*-axes in the proposed PM fiber when r_1 are 0.8 μm, 1.0 μm, 1.2 μm and 1.4 μm, where r_2=1.0 μm, Λ=3.4 μm and X=60 mol%

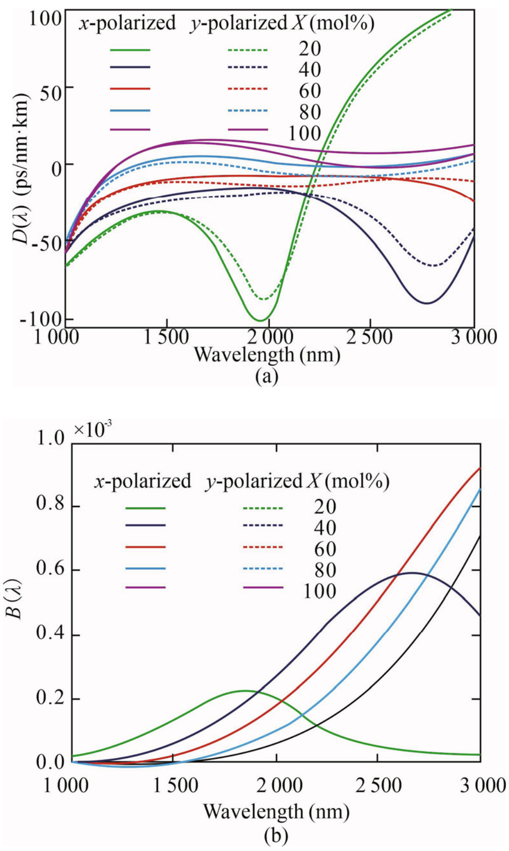

Fig.7 The curves of (a) GVD and (b) birefringence for FMs polarized along *x*- and *y*-axes in the proposed PM fiber with *X* values of 20 mol%, 40 mol%, 60 mol%, 80 mol% and 100 mol%, where r_1=1.2 μm, r_2=1.0 μm and Λ=3.4 μm

When the linearly polarized pulse is coupled into the PM fiber, we can define the angle of the polarization direction from *x*-axis as θ. When the input polarization is along two principal axes (θ=0° or 90°), only one of the orthogonally polarized modes is excited. In this case, Fig.9 shows the output pulses temporally and spectrally for different propagation lengths by solving the GNLSEs with the split-step Fourier method (SSFM)[21,23]. The pulses with both two polarization axes have a large spectral broadening at the propagation distance of 0.1 m, covering at the wavelengths ranging from 1 000 nm to 2 500 nm at −20 dB. When the pulses have a further propagation along the PM fiber, the spectral profiles nearly keep unchanged, while the temporal shapes continue to be broadened due to the GVD effect. For this reason, the propagation length is set to 0.5 m in the following discussion.

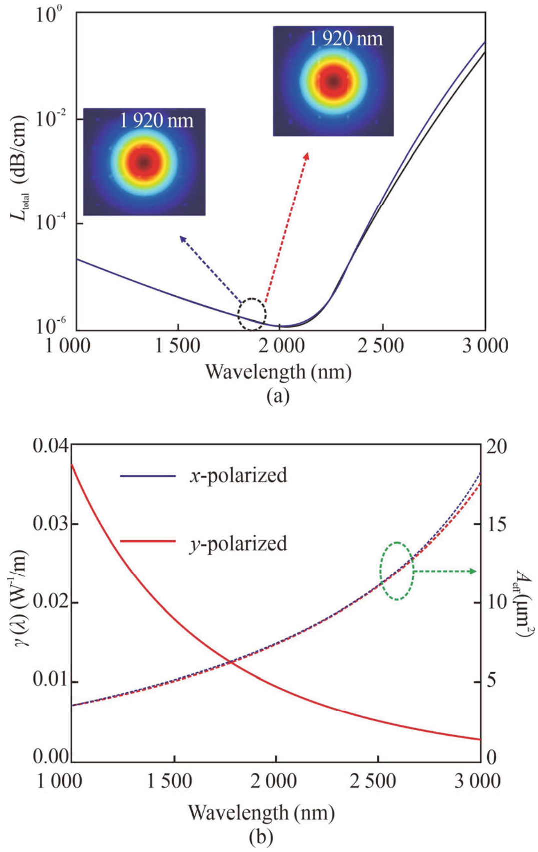

Fig.8 The curves of (a) total loss L_{total} and (b) the nonlinear parameter $\gamma(\lambda)$ (left) and effective mode area A_{eff} (right) of the FMs in the proposed PM fiber, where r_1=1.2 μm, r_2=1.0 μm, Λ=3.4 μm and X=60 mol%

As shown in Fig.10, when the 0.1 ps 1 920 nm pump pulses with different values of P_0 are coupled in the PM fiber along the principal axes, the output pulses show the smooth profiles temporally and spectrally. However, the input pulses polarized along the slow axis undergo relatively weaker GVD-induced pulse broadening, resulting in the broader output spectra compared with those of the pump pulse polarized along the fast axis. According to the report in Ref.[24], a tunable pulse with a peak power of 230 kW and a pulse width of 108 fs is generated near 2 μm. Thus, the peak power of pump pulse is adjusted from 50 kW to 150 kW in the numerical simulation. For example, when the 0.1 ps input pulse with 150 kW peak power is polarized along slow and fast axes, the spectral

Optoelectron. Lett. Vol.18 No.1

bandwidths at −20 dB of the output pulses are 1 700 nm (850—2 550 nm) and 1 550 nm (900—2 450 nm), respectively.

Furthermore, as shown in Fig.11, when the 100 kW pulses with different T_{FWHM} values are coupled into the PM fiber, the input pulse with T_{FWHM} =5 ps has a narrower spectrum compared with the 0.1 ps input pulse, which results in a relatively weaker GVD-induced pulse broadening in the temporal domain. For this reason, the output pulse in the former case has a peak power of 76 kW, which is much higher than that in the latter case. Moveover, in the case of T_{FWHM}=5 ps, the output pulses along both two principal axes temporally develop the oscillatory structures on the trailing edges mainly due to the new frequency components on the short wavelength side generated by the FWM effect.

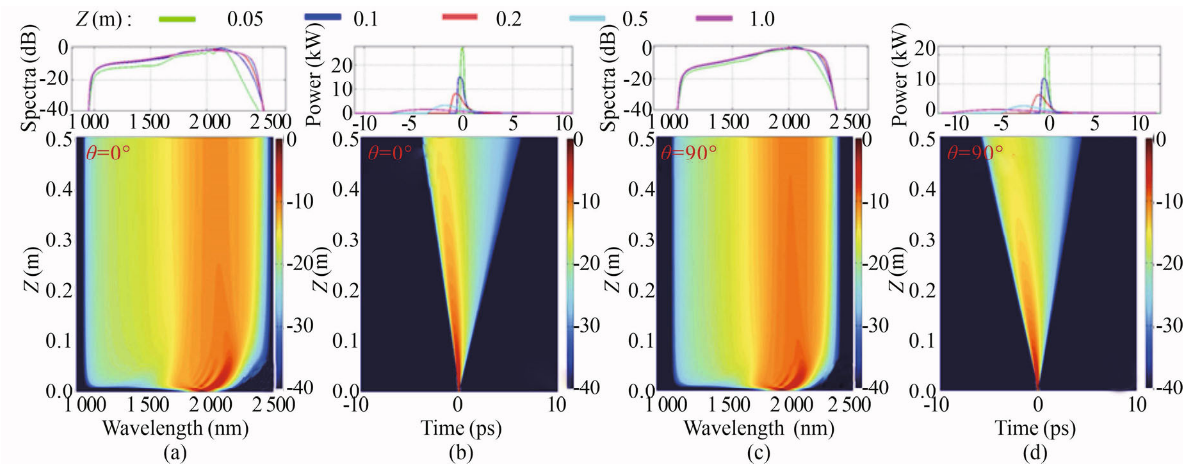

Fig.9 The output pulses polarized along (a)(b) slow and (c)(d) fast axes (b)(d) temporally and (a)(c) spectrally for different propagation lengths, where λ_0=1 920 nm, P_0=100 kW, T_{FWHM}=0.1 ps, r_1=1.2 μm, r_2=1.0 μm, Λ=3.4 μm and X=60 mol%

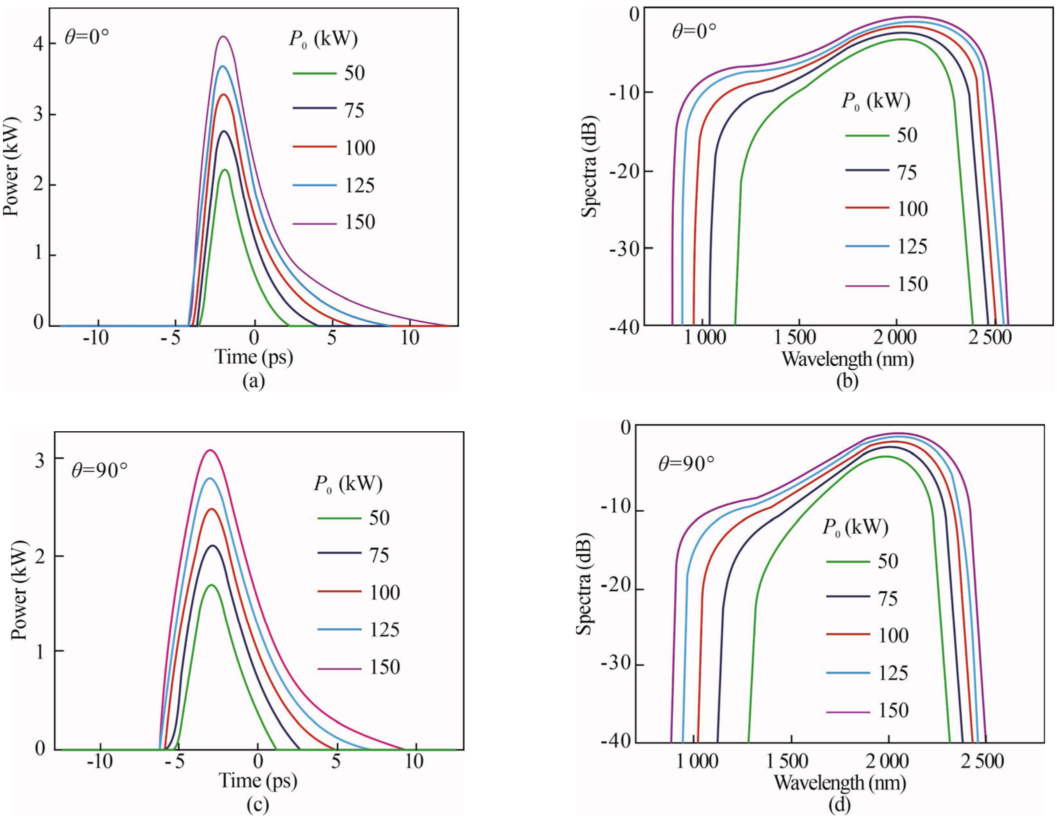

Fig.10 The output pulses polarized along (a)(b) slow and (c)(d) fast axes (a)(c) temporally and (b)(d) spectrally at the 0.5-m-long PM fiber end for the input pulses with different P_0, where λ_0=1 920 nm and T_{FWHM}=0.1 ps

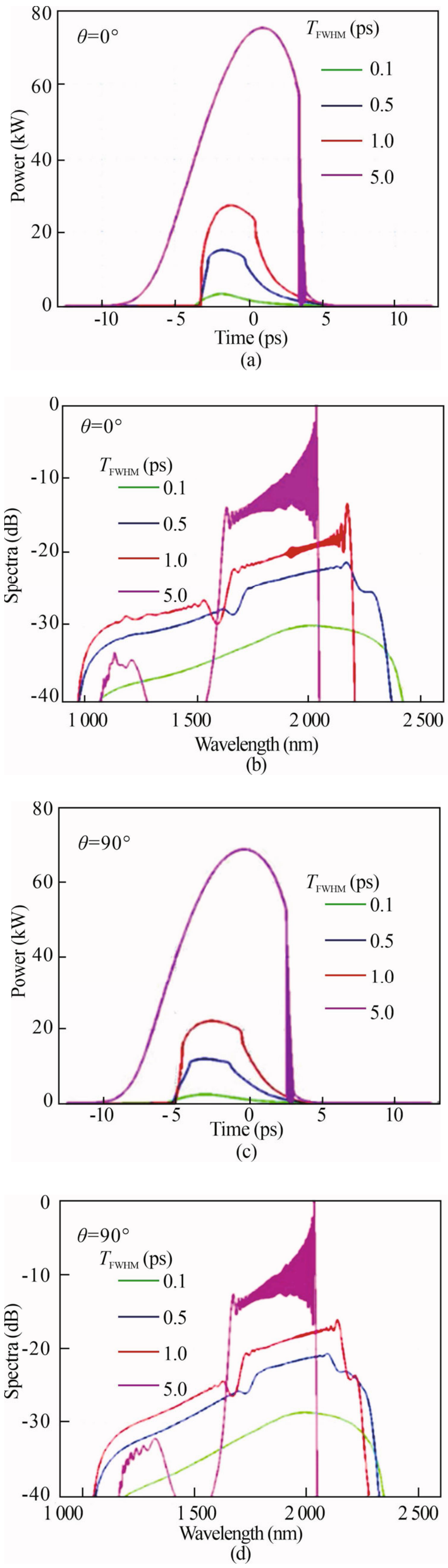

Fig.11 The output pulses polarized along (a)(b) slow and (c)(d) fast axes (a)(c) temporally and (b)(d) spectrally at the 0.5-m-long PM fiber end for the input pulses with different T_{FWHM}, where λ_0=1 920 nm and P_0=100 kW

As shown in Fig.12, the complex degree of first-order coherence $|g_{12}^{(1)}|(\lambda)$ can be obtained from an ensemble of 60 independently spectra[25], where the random quantum noise is added into the input pulse with one photon per mode. In the case with the input T_{FWHM} of 0.1 ps, the output pulses polarized along both two principal axes exhibit excellent coherence properties in the wavelength range of around 1 000–2 500 nm. However, the output pulses with input T_{FWHM} of 5 ps show a degradation of the coherence on the short wavelength side due to the new frequency components devoloped by the random quantum noise.

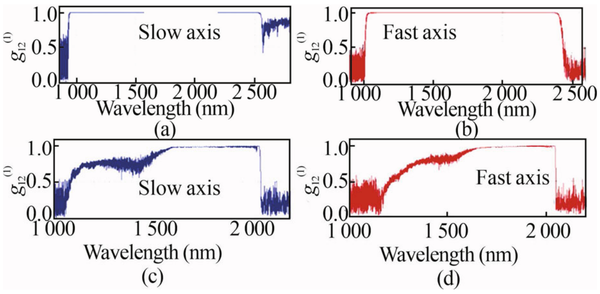

Fig.12 The degree of coherence $|g_{12}^{(1)}|$ of the pulse polarized along the slow and fast axes at the 0.5-m-long PM fiber end when (a)(b) T_{FWHM}=0.1 ps and (c)(d) T_{FWHM}=5 ps

The highly birefringent fiber in the 1 900 nm wavelength window can be demonstrated numerically by the PM fiber with heavily Ge-doped core and two side air holes in the cladding The proposed PM fiber with an proper choice of parameters has flatted normal GVD profile, high nonlinearity, low loss in the wavelength range from 1 000 nm to 3 000 nm. Furthermore, when the input polarization direction is along x or y axis of the PM fiber, the linearly polarized SC spectrum covering over one octave can be obtained in the wavelength range around 1 000—2 500 nm by using the 1 920 nm pump pulse with 0.1 ps duration and 100 kW peak power.

Statements and Declarations

The authors declare that there are no conflicts of interest related to this article.

References

[1] WANG C C, KIM J, JIN C, et al. Review：near infrared spectroscopy in optical coherence tomography[J]. Journal of near infrared spectroscopy, 2012, 20(1)：237.

[2] LABRUYÈRE A, TONELLO A, COUDERC V, et al. Compact supercontinuum sources and their biomedical applications[J]. Optical fiber technology, 2012, 18(5)：375-378.

[3] TU H, BOPPART S A. Coherent fiber supercontinuum for biophotonics[J]. Laser & photonics reviews, 2013, 7(5)：628-645.

[4] LEVICK A P, GREENWELL C L, IRELAND J, et al. Spectral radiance source based on supercontinuum laser and wavelength tunable bandpass filter：the spectrally tunable absolute irradiance and radiance source[J]. Applied optics, 2014, 53(16)：3508-3519.

[5] HUANG C L, LIAO M S, BI W J, et al. Ultraflat, broadband, and highly coherent supercontinuum generation in all-solid microstructured optical fibers with all-normal dispersion[J]. Photonics research, 2018, 6(6)：601-608.

[6] LIU W, WU Y, QI L. The influences of dispersions on supercontinuum in photonic crystal fiber[J]. Journal of physics：conference series, 2021, 1846(1)：012071.

[7] CHESHMBERAH A, SEIFOURI M, OLYAEE S. Supercontinuum generation in PCF with $As_2S_3/Ge_{20}Sb_{15}Se_{65}$ chalcogenide core pumped at third telecommunication wavelengths for WDM[J]. Optical and quantum electronics, 2020, 52(12)：509.

[8] MARIUSZ K, DAMIAN M, GRZEGORZ S, et al. Coherent supercontinuum generation in tellurite glass regular lattice photonic crystal fibers[J]. Journal of the optical society of America B, 2019, 36(2)：A112.

[9] HOANG V T, KASZTELANIC R, FILIPKOWSKI A, et al. Supercontinuum generation in an all-normal dispersion large core photonic crystal fiber infiltrated with carbon tetrachloride[J]. Optical materials express, 2019, 9(5)：2264.

[10] WANG C C, WANG M H, WU J. Heavily germanium-doped silica fiber with a flat normal dispersion profile[J]. IEEE photonics journal, 2015, 7(2)：1-10.

[11] LIU Y, ZHAO Y, LYNGSO J, et al. Suppressing short-term polarization noise and related spectral decoherence in all-normal dispersion fiber supercontinuum generation[J]. Journal of lightwave technology, 2015, 33(9)：1814-1820.

[12] TARNOWSKI K, MARTYNKIEN T, MERGO P, et al. Polarized all-normal dispersion supercontinuum reaching 2.5 μm generated in a birefringent microstructured silica fiber[J]. Optics express, 2017, 25(22)：27452-27463.

[13] GENIER E, GHOSH A N, BOBBA S, et al. Cross-phase modulation instability in PM ANDi fiber-based supercontinuum generation[C]//Conference on Lasers and Electro-Optics Europe：QELS_Fundamental Science, May 10-15, 2020, Washington, DC, United States. New York：IEEE, 2020：88-125.

[14] DOBRAKOWSKI D, RAMPUR A, STEPNIEWSKI G, et al. Development of highly nonlinear polarization maintaining fibers with normal dispersion across entire transmission window[J]. Journal of optics, 2018, 21(1)：015504.

[15] GHOSH A N, MENEGHETTI M, PETERSEN C R, et al. Chalcogenide-glass polarization-maintaining photonic crystal fiber for mid-infrared supercontinuum generation[C]//2019 Conference on Lasers and Electro-Optics Europe & European Quantum Electronics Conference (CLEO/Europe-EQEC), June 23-27, 2019, Munich, Germany. New York：IEEE, 2019.

[16] COUTURE N, OSTIC R, REDDY P H, et al. Polarization-resolved supercontinuum generated in a germania-doped photonic crystal fiber[J]. Journal of physics：photonics, 2021, 3(2)：25002.

[17] WANG C C, LI H W, QIAO Y J, et al. Normal-dispersion CS_2-filled silica fiber with broadband single-polarization property[J]. Optical fiber technology, 2021, 66：102665.

[18] FLEMING J W. Dispersion in GeO_2-SiO_2 glasses[J]. Applied optics, 1984, 23(4)：4486-4493.

[19] YURI Y, ALEXEI M. D-scan measurement of nonlinear refractive index in fibers heavily doped with GeO_2[J]. Optics letters, 2007, 32(22)：3257-3259.

[20] LAGSGAARD J, TU H H. How long wavelengths can one extract from silica-core fibers?[J]. Optics letters, 2013, 38(21)：4518-4521.

[21] AGRAWAL G P. Nonlinear fiber optics[M]. 4th ed. New York：Academic Press, 2007.

[22] ROTTWITT K, POVLSEN J H. Analyzing the fundamental properties of Raman amplification in optical fibers[J]. Journal of lightwave technology, 2005, 23(11)：3597-3605.

[23] RIEZNIK A A, HEIDT A M, KONIG P G, et al. Optimum integration procedures for supercontinuum simulation[J]. IEEE photonics journal, 2012, 4(2)：552-560.

[24] IMESHEV G, FERMANN M E. 230-kW peak power femtosecond pulses from a high power tunable source based on amplification in Tm-doped fiber[J]. Optics express, 2005, 13(19)：7424-7431.

[25] DUDLEY J M, GENTY G, COEN S. Supercontinuum generation is photonic crystal fiber[J]. Review of modern physics, 2006, 78：1135-1184.